



X-Ray Computed Tomography Analysis of Magnetically Oriented Short Steel Fibers and their Effect on Uniaxial Tensile Strength of Cement Mortar

Austin Rowan¹; Filmon G. Ghebreyesus²; Sina Zamen³; Lisa J. Willis⁴; Harold S. Halliday⁵; and Ehsan Dehghan-Niri, Ph.D.⁶

Abstract: The main objective of this study is to quantitatively determine the magnetic field capability of a Helmholtz coil in orienting steel fibers and show the correlation between the fiber orientation and tensile strength of steel fiber-reinforced concrete (SFRC) materials. Using X-ray computed tomography (CT), the exact distribution of fiber orientations was computed for both the magnetized and nonmagnetized samples containing 3, 5, 7, and 9 mm long fibers. The probability of a fiber being aligned parallel to the length of the specimen increased by 28.33%, 44.05%, 49.33%, and 27.12% for fibers with lengths of 3, 5, 7, and 9 mm, respectively. Finally, the uniaxial tensile strength of each sample was determined using direct tension tests. The average tensile strengths of the samples increased 0.51, 0.46, 0.64, and 0.76 MPa for the 3, 5, 7, and 9 mm fiber lengths, respectively. On average, the tensile strength of the samples increased by 27% after being exposed to an external magnetic field. **DOI:** 10.1061/(ASCE)MT.1943-5533.0004094. © 2021 American Society of Civil Engineers.

Author keywords: Short steel fiber-reinforced cementitious composites; Steel fibers; Magnetic field; Aligned steel fibers; X-ray computed tomography; Uniaxial tensile strength.

Introduction

Characterized by its ability to carry high compressive loads, durability, and workability, concrete is an extremely versatile material in the construction industry (Darwin et al. 2016). It is formed by mixing fine and coarse aggregates and water with cement (e.g., portland cement) and is set to cure over time. Ideally, the concrete should have a uniform distribution of aggregate sizes to eliminate any voids. Over time, the concrete gains strength as the hydration continues.

In the last few years, extensive studies have been conducted to improve concrete strength (Graybeal 2006; Wille et al. 2012; Zhang et al. 2014a, b, 2019). However, increased strengths have invariably been accompanied by brittle failure, which limits the application of high-strength concrete in construction. Because concrete on its own performs poorly when exposed to tensile loads, reinforcement is

¹M.S. Student, Dept. of Civil Engineering, New Mexico State Univ., 1040 S Horseshoe St., Las Cruces, NM 88003. Email: arowan@nmsu.edu ²M.S. Student, Dept. of Civil Engineering, New Mexico State Univ., 1040 S Horseshoe St., Las Cruces, NM 88003. Email: filmon@nmsu.edu

³Ph.D. Candidate, Dept. of Civil Engineering, New Mexico State Univ., 1040 S Horseshoe St., Las Cruces, NM 88003. ORCID: https://orcid.org/0000-0002-3235-5805. Email: szamen@nmsu.edu

⁴Metrology Lab Coordinator, Center for Advanced Manufacturing, Navajo Technical Univ., Lowerpoint Rd. State Hwy. 371, Crownpoint, NM 87313. ORCID: https://orcid.org/0000-0002-1856-933X. Email: l.willis@student.navajotech.edu

⁵Center for Advanced Manufacturing Coordinator, Center for Advanced Manufacturing, Navajo Technical Univ., Lowerpoint Rd. State Hwy. 371, Crownpoint, NM 87313. Email: hhalliday@navajotech.edu

⁶Assistant Professor, Dept. of Civil Engineering, New Mexico State Univ., 3035 S Espina St., Las Cruces, NM 88003 (corresponding author). ORCID: https://orcid.org/0000-0001-6839-4585. Email: niri@nmsu.edu

Note. This manuscript was submitted on March 18, 2021; approved on June 23, 2021; published online on November 26, 2021. Discussion period open until April 26, 2022; separate discussions must be submitted for individual papers. This paper is part of the *Journal of Materials in Civil Engineering*, © ASCE, ISSN 0899-1561.

added to compensate for this deficiency. When reinforcement is added, the concrete becomes a composite material, with the concrete providing compressive strength and the reinforcement providing tensile strength. Rebar is typically used as a reinforcement (Darwin et al. 2016). In some situations, it is beneficial to add composite fibers to concrete mixtures. While the rebar is ideal for carrying large tensile loads, short fibers, whether steel or some other material, are added to prevent the formation of smaller cracks. All concrete has microcracks formed because of thermal expansion, drying shrinkage, or applied load. Short fibers can also be used to prevent the growth of microcracks (Chen et al. 2020). For further study, interested readers can refer to the following papers (Chu and Kwan 2019; Kwan and Chu 2018).

In the last four decades, steel fiber-reinforced concrete (SFRC) has been the focus of several research projects (Groeneveld et al. 2017; Kang and Kim 2011; Yoo et al. 2016), and the incorporation of a large number of short steel fibers in ultrahigh-performance fiber-reinforced concrete (UHPFRC or UHPC) has resulted in both its high strength and ductility (Yoo et al. 2014). The addition of steel fibers to concrete can improve strength and durability, prevent the development and establishment of cracks, and also influence the bleeding content of concrete (Barnett et al. 2010; Chen et al. 2020; Reddy et al. 2013). Owing to its excellent postcracking ductility under tension and flexure, UHPC has been used in civil infrastructure where bending prevails. However, its unique tensile behavior is affected by many factors, such as fiber properties (e.g., strength, Poisson's ratio, stiffness, shape, geometry, and volume fraction), matrix properties (e.g., strength, Poisson's ratio, and stiffness), fiber distribution characteristics, fiber alignment, and fiber interface properties (Kang and Kim 2011; Laranjeira et al. 2011; Yoo et al. 2014). Typically, UHPC exhibits compressive strengths ranging from approximately 120-175 MPa and tensile strength of approximately 1 MPa (Graybeal 2006; Wille et al. 2012). The experimental results showed that UHPC has substantially higher compressive strength than tensile strength. This low tensile capacity makes concrete extremely susceptible to cracking and even failure when placed under extreme tensile loads.

It was recently shown that the orientation or alignment of steel fibers could further improve the mechanical properties of SFRC. Most importantly, the tensile behavior of SFRC is affected by the orientation of fibers. With a more favorable orientation of steel fibers, the ultimate strength and postpeak strength increase (Barnett et al. 2010). It was also shown that the fiber orientation could influence the bending and tensile behaviors of fiber-reinforced concrete (FRC) by increasing the fiber efficiency to bridge cracks (Xue et al. 2018). A study by Yoo et al. (2016) showed that the strength of cement was proportional to the ratio of fibers used. They showed that the tensile strength could be increased by increasing the fiber volume. Another study by Li et al. (2018) considered the influence of fiber orientation on the water permeability of FRC structures. It was shown that when the fiber orientation becomes less favorable, the first crack load, ultimate load, and tensile strength of tie specimens decrease (Li et al. 2018; Mu et al. 2017). The performance of fibers in material under tension is probably the broadest and simplest case. The load-carrying (tensile stress) ability is high when fibers are oriented parallel to the tensile stress, whereas perpendicular fibers may restrain lateral movement because of Poisson effects but do not contribute to the load-carrying ability (Groeneveld et al. 2017). The pre and postcracking behaviors of SFRC tensile specimens were modeled and experimentally investigated by Kang and Kim (Kang and Kim 2011). The specimens were cast so that the fibers were primarily aligned either perpendicular or parallel to the loading direction. The first cracking stress was approximately 10% higher for parallel fibers. After the cracks opened, the fibers were involved in crack bridging, and the effects of fiber orientation were more significant. The maximum stress reported was 40% higher for parallel fibers (Kang and Kim 2011).

Recently, there have also been extensive studies looking at the performance of cement containing both steel fibers and nano-SiO₂ particles. In particular, three studies by Peng Zhang et al. were performed to evaluate the performance of cement in various categories containing both steel fibers and SiO₂ (Zhang et al. 2014a, b, 2019). It was shown that the addition of less than 5% nano-SiO2 increased the tensile strength. When nano-SiO₂ content was increased above 5%, the flexural strength, as well as the flexural modulus, decreased. They also observed that adding steel fibers increased flexural strength and the modulus of elasticity when the steel content was below 2% (Zhang et al. 2014b). In another study by Peng Zhang et al., the compressive strength of cement mortar containing both nano-SiO₂ and steel fibers was explored. As with the previous study, they found that compressive strength improved when the nano-SiO₂ content was below 5%. When the content exceeded 5%, the compressive strengths decreased. The study showed that with steel fiber contents ranging from 0.5% to 2.5%, the compressive strength of the samples increased with an increasing fiber content (Zhang et al. 2014a).

Fibers in concrete can be aligned using several mechanisms, such as by the drag force during the pouring of the concrete mixture. Yoo et al. (2014) used two different pouring methods to orient the fibers: (1) placing the cement at one end of the mold and allowing it to flow and to fill from the one end; and (2) placing cement paste at both ends and the center of the mold until the mold was full. According to their study, the first pouring method was more efficient in orienting the fibers. They also showed that oriented fibers increased the flexural strength capacity under impact loading scenarios (Yoo et al. 2016). The orientation of fibers in the SFRC can be influenced by compaction. When vibration is applied for compaction, the fiber orientation and distribution are affected

(Ciambella et al. 2017; Mortazavian and Fatemi 2015). In general, fibers tend to align in a horizontal plane. The placement method also has a strong effect on fiber orientation. The fiber orientation in round slabs, which were cast from the center and edge, was investigated by the authors of Barnett et al. (2010). Surprisingly, the fibers were aligned perpendicular to the flow of fresh concrete. Specifically, for panels cast from the center, the concrete flooded outward radially, and the fibers tended to be aligned in the hoop direction. This contrasts with Kim et al. (2008), who cast beam and slab specimens and observed fibers aligned parallel to the direction of flow. Likewise, for a fiber whose main axis is at the same angle as the direction of flow, the drag force on the fiber produces a moment that tends to cause the fiber to rotate (Groeneveld et al. 2017). The drag-induced moment is zero when the fiber is aligned with the direction of the flow. The contribution of mixing, flow, vibration, casting, and formwork geometry on the orientation of steel fibers in concrete was studied by Laranjeira et al. (2012). The effect of mixing depends on the rheological properties of the concrete. In a stiff, unflowable mix, fibers tended to randomly orient, whereas fibers in a flowable mix tended to align themselves in the direction of the flow more easily. Similarly, the direction, placement height, and flowability of concrete also affected the degree of alignment introduced during casting. The height from which concrete is placed (i.e., how far it drops into the formwork) affects the extent to which concrete placement disturbs it (Edgington and Hannant 1972; Laranjeira et al. 2012). The ability to control fiber alignment during construction can enhance concrete properties, such as tensile strength and durability.

Recently, Linsel proposed a method to orient ferromagnetic fibers using magnetic fields (Stähli et al. 2008). Based on the principle of magnetism, a magnetic force can be generated to rotate the steel fibers and vibrate the concrete. Because of the applied magnetic force, the steel fibers move and rotate in the same direction as the magnetic field (Villar et al. 2019a). It was demonstrated that the efficiency of reinforcing steel fibers could be substantially influenced by fiber orientation (Mu et al. 2017). The orientation efficiency factor, η , is defined as the ratio between the reinforcement of short-inclined fibers and the reinforcement of continuous fibers aligned to the load. This factor is used to indicate the efficiency of fiber reinforcement (Mu et al. 2017). When the fibers were aligned perpendicular to the load, the orientation efficiency factor was 0, and when the fibers were aligned in the direction of the applied tensile load, the factor was 1.0. An orientation efficiency between 1/6 and 1/2 can be found from the experimental test of ordinary steel fiber-reinforced concrete and 0.405 from a theoretical analysis (Villar et al. 2019a). Clearly, the tensile performance of the concrete will be improved significantly if the orientation of short steel fibers can be aligned parallel to the tensile stress of the concrete element (e.g., efficiency factor equal to 1) (Xue et al. 2018). Fibers composed of various polymer materials can also be used instead of steel fibers (Ciambella et al. 2017; Zhou and Uchida 2013).

Before one can evaluate the alignment effects on the mechanical performance of materials, the level of orientation must be determined. Microscopic techniques, such as X-ray computed tomography (CT), X-ray radiography, optical diffraction, and electron microscopy, can be used to investigate the orientation distribution of fibers (Juárez-Badillo 1999). However, the CT scan is the best nondestructive testing method for determining fiber orientation distributions. CT scans allow the viewer to physically see the inside of the samples, allowing for direct qualitative analysis. This does not allow for a simple method to quantitatively analyze the samples. Additional processing of the scans must be performed to obtain a precise evaluation of the fiber orientations. This study uses a mathematical method based on gradient information of fiber

geometry obtained from CT scans. With this information, the angle of each pixel associated with each fiber can be mathematically determined, and thus, the probability densities of each orientation angle can be computed.

The main objective of this study is to quantitatively determine the magnetic field capability to orient steel fibers using X-ray CT and to show the correlation between fiber orientation and tensile strength of composite cementitious materials. Section "Design of an Electromagnetic Coil" explains the design and setup of the Helmholtz coil used in this study. The third section covers the CT scanning results and the image analysis method used to determine the orientation distributions quantitatively. The fourth section contains the mix design and tensile strength experimental setup. The fifth section presents the results and discussion of the orientation analysis and tensile strengths of all the samples. Finally, the conclusions are presented in the section "Conclusions."

Design of an Electromagnetic Coil

Electromagnetic Generation

As mentioned before, a magnetic force can be used to align ferromagnetic fibers, such as steel fibers. The magnetic field intensity should be uniform in the fresh cement mortar region to align the steel fibers and avoid translational movements. Nonzero magnetic field gradients can result in translational movements, and consequently, the steel fibers can be concentrated and attracted at the place where the induction of the magnetic field is higher (Stähli et al. 2008). In other words, to be able only to rotate the fibers in a magnetic field, the gradient of the magnetic field must be negligible, and the magnetic field must be uniform. In a uniform magnetic field, steel fibers in fresh concrete are exposed to the following forces (Wijffels 2013): gravity, magnetic force, viscous resistance, and buoyancy. The forces acting in the vertical direction are gravity and buoyancy, which have no influence on the rotation of steel fibers. A steel fiber in a magnetic field can be defined as a dipole with positive and negative charges. The positive charge represents the north pole and is aligned with the direction of the magnetic field, which is direct from north to south. The magnetic force must be large enough to overcome the viscous resistance to align the steel fibers in a mix (Graybeal 2006; Mu et al. 2017; Wijffels 2013; Xue et al. 2018). A simplified theoretical model to explain the alignment of magnetic particles into a viscous fluid by a homogeneous magnetic field was given by Kimura et al. (2000) and Wijffels et al. (2017). Two forces, (1) the drag moment resistant force (T_d) , and (2) the acting rotational magnetic force (T_m) , were considered as the dominant forces acting on a single fiber. The T_m has to overcome the resistance force T_d before a single fiber can start rotating. The formulas for drag moment resistant force (T_d) are given in Eqs. (1) and (2)

$$T_d = L \frac{d\theta}{dt} \tag{1}$$

$$L = \frac{\pi \eta l^3}{3(\ln(2a_r) - \frac{1}{2})} \tag{2}$$

where $d\theta/dt$, η , l, w, and a_r = first derivative of angle (θ) between the long axis and the direction of the magnetic field with respect to time (t), the viscosity of the fluid, the length of the fiber, the diameter of the fiber, and the aspect ratio of the fiber, defined as l/w, respectively. Based on this model, as the fiber diameter and length increase, the viscous resistance increases. This means that a larger

diameter and longer fibers will require a stronger magnetic field for alignment.

On the other hand, when the fiber is short, the magnetic moment force acting on the fiber will not be as strong as the force acting on a longer fiber. Eqs. (3) and (4) determine the rotational moment (T_m) imposed by a uniform magnetic field B

$$T_m = v(\vec{M} \times \vec{B}) \tag{3}$$

$$v = \frac{4}{3} \left(\frac{w}{2}\right)^2 l \tag{4}$$

In Eq. (3), M represents the magnetization induced by the external magnetic field. Notice that the v term decreases with the decreasing length (l) and increases when the diameter (w) increases. Thus, the rotational force applied to a short fiber will be weaker when compared to the force acting on a long fiber. In contrary to the negative effect of a long fiber length and a large diameter on the alignment because of the increase in the resisting force, the magnetic rotational force will be stronger for fibers with a larger diameter and longer length. In addition, the simplified theoretical model does not consider complexities as a result of fiber-fiber interactions and the dynamic behavior of the fibers. In general, there are several contradicting and complex factors affecting the fiber alignment so that optimal parameters that better align a particular fiber to a uniform magnetic field cannot be easily determined theoretically.

In this study, a Helmholtz coil was used to generate a uniform magnetic field. This coil is named after German physicist Hermann von Helmholtz (Gyawali 2008). The principle of the coil is to produce a region with a nearly uniform magnetic field by having two identical circular electromagnetic coils placed symmetrically along a common axis, as shown in Fig. 1.

Design of a Helmholtz Coil

An electromagnetic coil consists of a conductive wire wound into either a coil or a helix shape. For the design, a copper wire is wound into a coil shape. When a current runs through the wire, a magnetic field is generated. To increase the magnitude of the magnetic field,

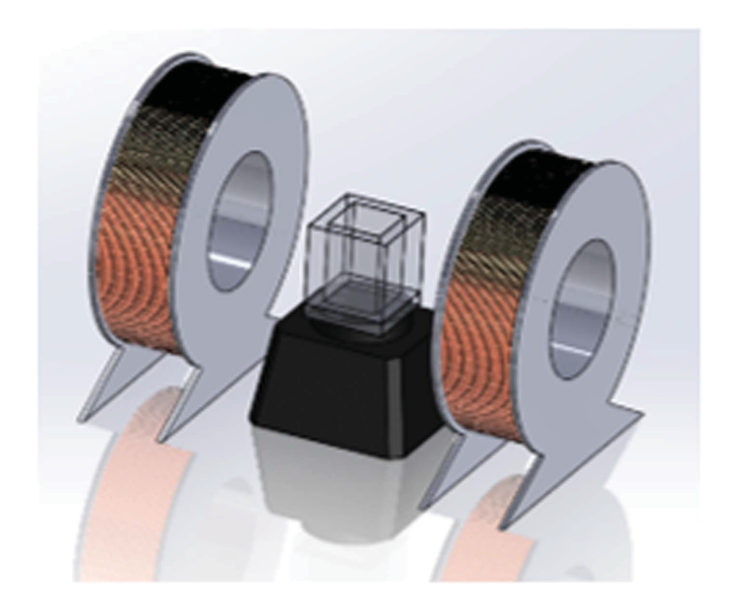


Fig. 1. Helmholtz coil.

another coil is placed parallel to the first, where the currents travel in the same direction (Edgington and Hannant 1972).

The equation detailed subsequently gives the exact value of the magnetic field at the center point between the two coils. The magnetic field B at the midpoint between the coils at x distance from each coil is given

$$B(x) = \frac{\mu_0 n I R^2}{(R^2 + x^2)^{3/2}}$$
 (5)

where B = magnetic flux density in Tesla (T); $\mu_0 =$ permeability of free space, which is equal to $4\pi \times 10^{-7}$ and has no dimension; n = number of turns; I = current in amperes; and R = radius of the coil in meters.

The initial configuration was designed using Eq. (1), together with the design flux density, physical properties of the copper wire, and boundary conditions. This is an iterative process in which a model is designed. It was initially decided to generate a magnetic flux density between 0.03 and 0.07 T. This range is based on other research papers in which a magnetic field was successfully used to orient steel fibers (Islam 2008). The output of the model consists of the magnetic flux density in the coil and a current power supply equal to 20 A, which is associated with the maximum capacity of our power supply.

Two pairs of identical coils were designed and manufactured with 400 turns, as shown in Fig. 2. A small shaker was placed between the two coils to facilitate fiber alignment. The distance between the coils is 254 mm (10 in.). These coils have an inner diameter of 101.6 mm (4 in.) and an outer diameter of 254 mm (10 in.). The DC power supply (CPX400DP Dual 420 W) has an output of 20 A at 120 V. With the specifications mentioned and using Eq. (1), the magnetic flux density was calculated to be 0.038 T for 20 A. In this equation, it is assumed that the coil width and height are significantly smaller than the coil diameter. However, this assumption is not exactly true in our case. Thus, to estimate the magnetic flux density, the average of the inner and outer radii of the coil and the inner distance between the coils were considered.

An AWG12 wire with a diameter of 2 mm was used to wind the Helmholtz coil to carry a maximum current of 20 A with a short period of exposure (e.g., less than 40 s) to avoid overheating. The temperature inside the coil was continuously monitored using an infrared thermometer during the experiment to avoid overheating. The magnetic flux density (B) at the center, between the coils, was measured using a Gaussmeter (Lutron 828, Taiwan). The magnetic flux density values were 0.024 and 0.048 T for currents of 10 A and 20 A, respectively. The magnetic field was relatively uniform

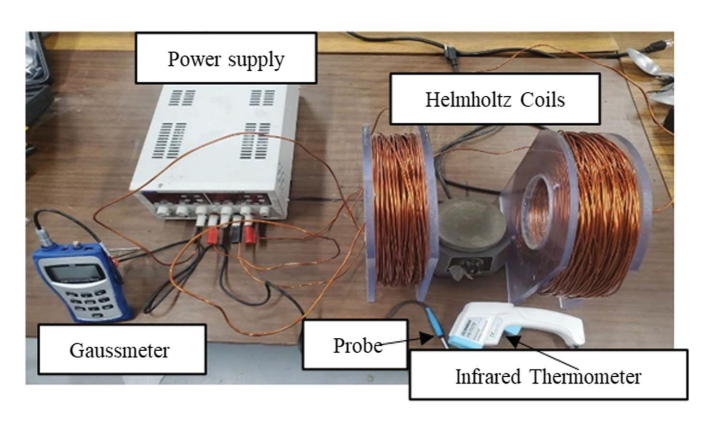


Fig. 2. Magnetization setup.

(alterations less than 5%) in the central area of the coils. This enabled us to impose the magnetic flux density necessary for orienting the fibers without translational movement. The earth's magnetic field was not shielded by this exposure device. Fig. 2 shows the coil, Gaussmeter, infrared thermometer, shaker, and power supply used in this study.

Orientation Distribution Analysis

X-Ray Computed Tomography

To capture the CT scans, an X3000CT 225 kV CT scanner manufactured by North Star Imaging (NSI) (Aliso Viejo, California) was used. The voltage and current settings were 116 kV and 205 μA , respectively, with a focal spot size of 23.78 microns. The settings used for the scans provided a 3.23 magnification and a voxel size of 39.4 microns. A total of 2,200 images were taken over 360° of rotation. The radiographs were reconstructed using the NSI efXct reconstruction software, and the reconstructed volume was imported to Volume Graphics software to acquire a complete volume and image stacks. For additional information regarding CT scanning, readers can refer to the study by Subburaj (2012).

Quantitative Orientation Analysis Using CT Scans

Determining the local orientation of fibers and their distribution are addressed in this section. The method used could provide local angle information at every pixel that correlates to a fiber. This information is useful for quantitative analysis of the CT scans. Each sample's orientation distribution could easily be correlated with their respective tensile strengths, making the relationship between them obvious.

Fig. 3(a) shows the histogram associated with the CT scan shown in Fig. 3(b). Note that this scan has already been used as a threshold by trial and error until only the fibers are visible. To do this, the lower and upper bounds were adjusted to include only the pixels associated with the fibers of the sample. This process was applied to each sample. As seen in Fig. 3(b), it is effective in processing the CT data.

Using the given North Star Imaging (NSI) volume-viewing software (version efX-CT Lite) and histogram information, the fibers were isolated from the surrounding cementitious material and exported as two-dimensional projected images resulting from threedimensional CT scans. It is important to note that the projection of three-dimensional CT scans into one vertical plane was used in our orientation analysis. When the local pixel angles were computed, they were only calculated for the x-z plane (using simple Cartesian coordinates). For a more robust analysis of the orientation of the fibers, the angles for both the x-z and y-z planes should be calculated. Comparing the analysis results of different vertical projections (e.g., x and y), it was concluded that with less computational effort, the two-dimensional analysis of a single vertical projection provided an adequate representation of the distribution of fibers suspended within the cement mortar. Therefore, only one projection from the x-face of each sample was used for the distribution analysis. These images were saved in a binary form to make the computation more efficient.

Because thousands of images must be processed, a computationally efficient algorithm is needed to calculate the orientation of each pixel. Püspöki et al. (2016) provided an extremely useful overview of various techniques used to compute the orientation information of pixels. All such methods rely heavily on differential and convolution operators. The simplest and earliest methods rely mostly on the gradient information of an image. The gradients of

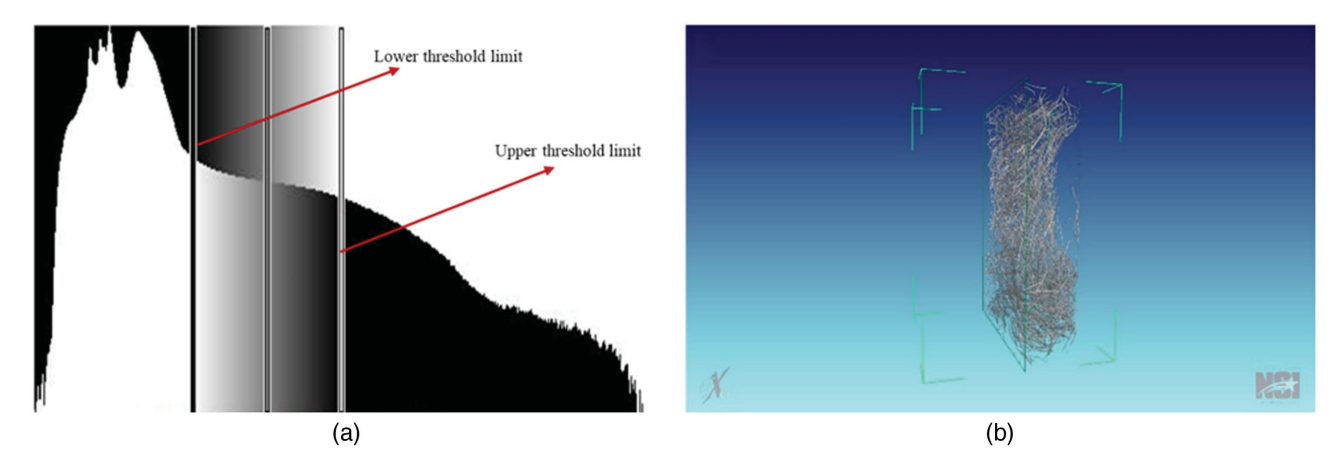


Fig. 3. (a) Volume histogram; and (b) volume space sliced through the middle for viewing purposes.

an image detect any edges in an image, or rather the direction of the most rapid change. The gradient then points in the *steepest* direction. This was done in both the x and y directions of the image, finding the strongest edges in both directions. To find the gradient of an image, the partial first derivatives must be taken with respect to both the x and y directions. With this, the angle of each pixel can be determined by simply dividing the arctangent of the y-gradient by the x-gradient (Püspöki et al. 2016).

A gradient-based analysis is popular because it can be easily implemented. The use of derivatives can be made more robust when using a structure tensor (Püspöki et al. 2016). For a two-dimensional analysis, the structure tensor at pixel x_0 is defined

$$J(x_0) = \int w(x - x_0)(\nabla f(x))(\nabla^T f(x_0)) dx_1 dx_2 \tag{6}$$

where w = Gaussian kernel. Gaussian kernels (Gonzalez and Woods 2008) were used to smooth the image, thus reducing the effects of noise. The $\nabla f(x_0)$ represents the gradient of pixel x_0 , where ∇ represents the gradient operation. The 2 × 2 structure tensor computed at every pixel is then determined by smoothing the following

$$J = \begin{bmatrix} f_x^2 & f_x f_y \\ f_y^2 & f_x f_y \end{bmatrix} \tag{7}$$

where f_x and $f_y = x$ and y gradients of the image, respectively (Püspöki et al. 2016).

After the structure tensor is computed, the local orientation (θ) of each pixel can be determined using the following equation

$$\theta = \frac{1}{2}\arctan\left(2 \times \frac{f_x f_y}{f_y^2 - f_x^2}\right) \tag{8}$$

For the purposes of this paper, theta (θ) is defined as the angle between the horizontal axis and the vertical direction, where the vertical direction represents the direction of the magnetic field. Thus, an angle calculated as 90° corresponds to a pixel that was oriented with the direction of the magnetic field. This angle was calculated as previously described.

Initially, this algorithm was implemented in this study using Python software (Lutz 2013). Python worked well for small-scale computations but became sluggish when orientation distributions for thousands of images had to be calculated. As a remedy to this, it was found that the OrientationJ plugin for ImageJ was much faster and more efficient. ImageJ is an open-source, java-based image processing program used for several scientific research

purposes. It is also highly extensible, meaning that several addon packages can be added to it. In this study, OrientationJ was ideal for computing fiber orientation. OrientationJ computes the structure tensor at every pixel using the gradient information of an image, using the process already described. This was performed for each two-dimensional image obtained from three-dimensional CT scans. Using OrientationJ, a histogram was calculated using the frequency of each angle in the image. The individual projections were then added together to form a histogram of the entire CT scan. Then, the probability density function (PDF) was calculated for the local angles. In addition, a heat map was constructed to visualize the distribution of angles within the fibers.

Orientation Calculates the angles within the range of -90° to 90° from the vertical axis. To make the analysis more straightforward, the absolute value of the -90° angle was taken and added to the angles that were already positive. This allowed all pixels associated with the oriented fibers to be grouped together. It is important to note that only one vertical plane resulting from the projection of each three-dimensional CT scan was used in this study. We concluded this to be sufficient for showing the correlation between the magnetic field, tensile strength, and fiber orientation.

Experimental Setup

This section presents the details of the concrete mixture that was used with the proportions to test the effects of fiber orientation on SFRC materials and the process used in magnetization. A spreadflow test was performed according to ASTM C1437 (ASTM 2007) after testing each mixture. Finally, a direct tension test and X-ray CT scans were performed on magnetized and nonmagnetized SFRC specimens to determine the fiber orientation.

Mixture Proportions and Fibers

A normal concrete mixture comprising Type I portland cement, water, sand (No. 30 sieve), and 1% steel fibers by volume was used in this study. Sand and cement were obtained from local sources. After the mixing process, the concrete paste was cast using two cylindrical plastic molds (Fig. 3). To create a weaker area in the middle of the sample (i.e., create a neck shape), a three-dimensional (3D) printed plastic neck with an outside height of 38.1 mm, inside height of 25.6 mm, outside diameter of 50 mm, and an interior diameter of 37.6 mm was used (Fig. 4). The concrete was rodded 25 times at every increment. After filling half of the mold, the neck was inserted, and the remaining half was filled with a concrete mix

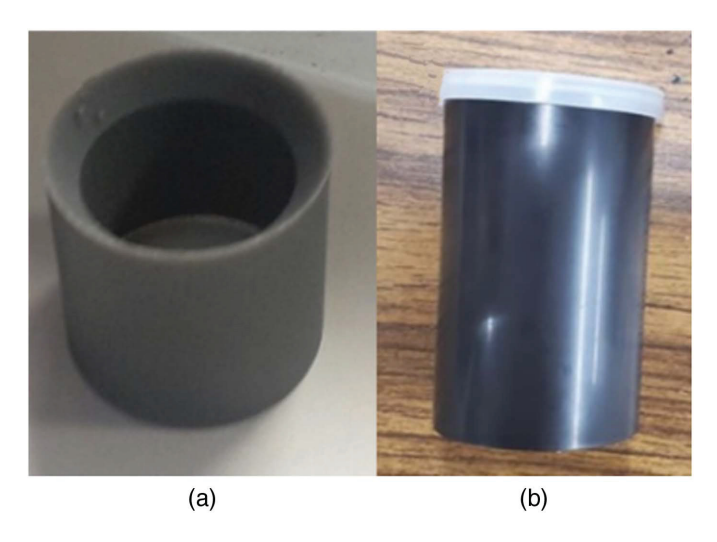


Fig. 4. Tensile molds: (a) plastic neck; and (b) cylindrical molds.

Table 1. Tensile sample mix proportions

Material	kg/m^3	(lb/yd ³)
Cement	385	650
Sand	530	900
Water	154	260
Steel fiber	44	75

until filled flush. Plastic molds and necks were used to avoid electromagnetic interference during the concrete magnetization. Table 1 lists the mixture proportions by volume used to cast the concrete samples. This mix design was used for a previous study using an external magnetic field to orient fibers in cement mortar (Mu et al. 2017). In addition, the paste volume used was checked using the methodologies given by Chu (2019).

The fibers used to reinforce the cement were 3, 5, 7, and 9 mm long. The diameter of each fiber length was 0.2 mm, implying aspect ratios of 1:15, 1:25, 1:35, and 1:45, respectively. The use of the aforementioned fiber lengths and diameters is typical of the materials used in SFRC.

In order to show the general state of the cement when it was poured, a flow table test in accordance with ASTM C1437 (ASTM 2007) was performed. The apparatus contained a standard cone mold with a 69.85 mm top diameter and 101.6 mm bottom diameter and a flow table with a 254-mm diameter. The results from the spread-flow test are given in Table 2.

Magnetization Process

In this study, steel fibers of four different lengths (3, 5, 7, and 9 mm) were considered. In the concrete mixture for every fiber length, two 101 mm long (4-in.) and 51 mm (2-in.) diameter cylindrical samples were cast. A small Hobart benchtop mixer was used to mix the materials. A constant procedure was performed for all the mixes. According to the respective mix design and the desired number of samples, each constituent was weighed before the mixing process. To begin the mixing process, the dry materials were poured into a small mixer. As a first step, dry mixing took place for approximately 50 s, and then water was added to the mixture and mixed until all materials were uniformly mixed. After obtaining a thorough mix, steel fibers were added and mixed for approximately 2 min. A spread-flow test was set up for testing after

Table 2. Flow table results for each cement sample

Fiber length (mm)	Test No.	Front to back (mm)	Left to right (mm)	Diagonally (mm)
3	1	122.4	127.8	138.9
	2	123.5	134.5	139.9
	3	122.5	136.1	143.5
5	1	124.5	134.2	140.3
	2	123.3	135.2	141.8
	3	122.3	135.1	142.8
7	1	124.1	135.7	142.5
	2	123.5	136.2	142.3
	3	121.8	135.3	142.9
9	1	123.1	136.3	142.4
	2	122.9	136.2	142.4
	3	122.7	135.8	143.9
Average	_	123.05	134.8	141.9

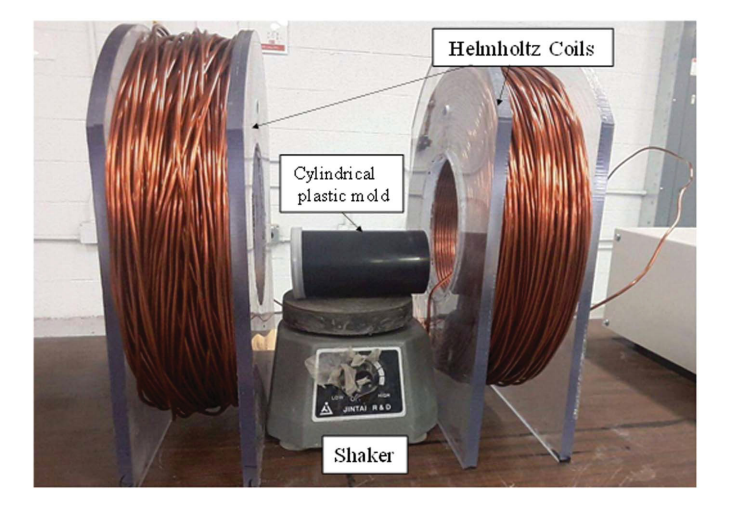


Fig. 5. Magnetization setup after casting samples.

completing the mixing procedure. The concrete was rodded 25 times

at every increment. After filling half of the mold, the neck was inserted, and the remaining half was filled with a concrete mix until filled flush. Plastic molds and necks were used to avoid electromagnetic interference during the concrete magnetization. One sample was magnetized for 40 s using a 20 A current, and the other sample was not exposed to the magnetic field. Both magnetized and nonmagnetized samples were placed horizontally on a small shaker to facilitate fiber alignment. The magnetized and nonmagnetized samples experienced the same level of vibration.

The building and magnetization processes used to cast the tensile samples are shown in Fig. 4.

Direct Tensile Test

Direct tensile strength was determined in accordance with ASTM C1583 (ASTM 2013) for this study (Garcia 2019). The direct tension tests were conducted after 7 days of curing in hot water and placed in an oven at a temperature of 95°C (203°F). Tensile tests were carried out soon after all the preparations were completed. Fig. 5 shows the tensile specimen with a 3D printed neck and the weak area of the specimen.

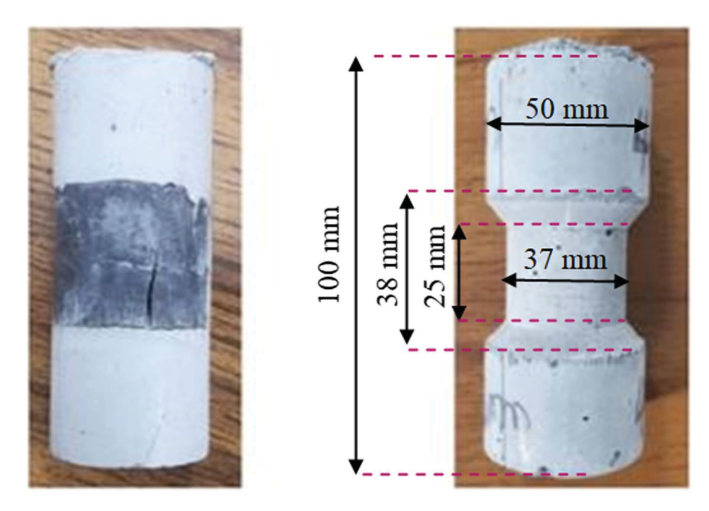


Fig. 6. Tensile strength specimens.

The specimen was placed on the tensile strength apparatus, and the two steel end plates that were epoxied and attached to the specimen were fixed to the upper and lower heads (eye bolts) of the testing machine (Villar et al. 2019b). Concentric loading was confirmed when the eyebolts served as pivots at both ends of the specimen during loading. Fig. 6 illustrates the attachment of the eyebolts to the endplates epoxied to the specimen. As expected, the samples were completely broken from the middle. Finally, a grinder was used to remove the epoxy material from the steel plate to reuse the metal plates for the other samples.

Results and Discussion

During the curing process, the fibers were oriented to flow parallel to the length of the samples by exposing them to an external magnetic field. The orientation distributions were qualitatively and quantitatively analyzed. For a qualitative analysis of the orientations, local pixel orientations were assigned to a color map, thereby creating a heat map in which red corresponds to perpendicular to the horizontal (parallel to magnetic field direction) axis and turquois corresponds to parallel with the vertical axis. This means that all red pixels are representative of any pixels aligned with the magnetic field. The color bar was created using OrientationJ of ImageJ software. The qualitative analysis provides easy visualization of the data. The arrow on the oriented distributions indicates the direction of the magnetic field.

In this paper, the oriented degree is defined as the angle between the horizontal axis and the vertical direction, where the vertical direction represents the direction of the magnetic field. Thus, an angle calculated as 90° corresponds to a pixel that was oriented in the direction of the magnetic field. This angle was calculated as previously described in the section "Quantitative Orientation Analysis Using CT Scans."

Fig. 7 shows the CT images of both the magnetized and non-magnetized samples. In this figure, the oriented distributions correspond to the magnetized samples. The heat maps show that there is a distinct difference between the magnetized and nonmagnetized cases. It is easy to observe that the nonmagnetized samples have a larger spectrum of colors, mostly falling within a $\pm 15^{\circ}$ range at around 45°. A very small proportion is red, meaning that most fibers are not oriented parallel to the length of the sample. In contrast, as we expected, it can be observed from the magnetized samples that

most of the fibers had aligned with the magnetic field. Nearly every pixel associated with fibers was red, while the rest appeared to be within $\pm 15^{\circ}$. The qualitative analysis is a quick and easy way to show that the fibers exposed to a magnetic field are effectively aligned with the direction of the magnetic field.

When placed into the molds, the fibers tended to align parallel to the mold boundaries. This is evident from the heat maps of each specimen. The nonmagnetized specimens had fibers that were initially aligned parallel with the length of the specimen. Most of these were observed to be outside the specimens (e.g., close to the boundary of the mold). Another factor affecting the initial orientation of the fibers is the pouring method used. When poured, the fibers tended to align in the pour direction. Inevitably, there will be variations in how each sample is prepared. These variations will change how the fibers are initially oriented while being mixed and poured.

The tendency of the fibers to align parallel to the length of the sample means the nonmagnetized fibers cannot be referred to as having a random distribution. For a truly random distribution of fibers, it would be expected that the PDF curves for the nonmagnetized samples would follow a flat distribution. However, as shown in Fig. 8, the curve for the nonmagnetized samples is asymmetrical about the 45° axis.

The orientation probability density functions for the nonmagnetized and magnetized fibers were plotted for each fiber length. This provides a quantitative way of analyzing the orientation distribution as well as the susceptibility of each fiber length. Once the level of orientation is determined, it can be used to determine its correlation with the corresponding tensile strengths.

Fig. 8 shows the probability density functions for each fiber length. The dotted lines represent the distribution with no applied magnetic field, and the solid lines are the plots associated with the magnetized samples. The x-axis ranges from 0° to 90° , where 90° corresponds to the vertical axis parallel to the magnetization direction, and the y-axis is the probability density. The gray cylinders represent the fiber orientation at 0°,45°, and 90°. Each plot represents the cumulative sum of each two-dimensional (2D) slice on the CT scan. The PDFs were then calculated by normalizing each histogram, as described previously. Normalization was performed by dividing the individual frequency of each angle by the total number of pixels. It is important to note that all the angles calculated as negative were considered positive. This was done to show how pixels were oriented in the same direction as the magnetic field, which was 90° from the horizontal axis. When looking at the nonmagnetized PDFs, initially, they all start with a higher probability of between 0° and 45°. After magnetization, all plots show a decrease in the PDF at 45° within approximately $\pm 15^{\circ}$. In the range of 45°-90°, the PDF value of the nonmagnetized case is below the magnetized one indicating the fibers aligned to the direction of the magnetic field. In addition, notice how the magnetized cases have a smoother distribution until 90°. At 90°, there is a large spike and increase in the PDF value, indicating a higher probability of pixels being oriented with the magnetic field.

Looking at only the 90° oriented pixels, the magnetized pixels had a higher probability of being perfectly aligned with the magnetic field. While the nonmagnetized samples had a slight spike at approximately 90°, it was negligible when compared to the magnetized samples for every fiber length. The probability of 3-mm fibers oriented along the vertical axis increased from 0.039 to 0.084, 5-mm fibers increased from 0.028 to 0.085, 7-mm fibers increased from 0.029 to 0.085, and 9-mm fibers increased from 0.025 to 0.075.

Because the fibers oriented between 45° and 90° carry loads more effectively than those that are not, the probability of having

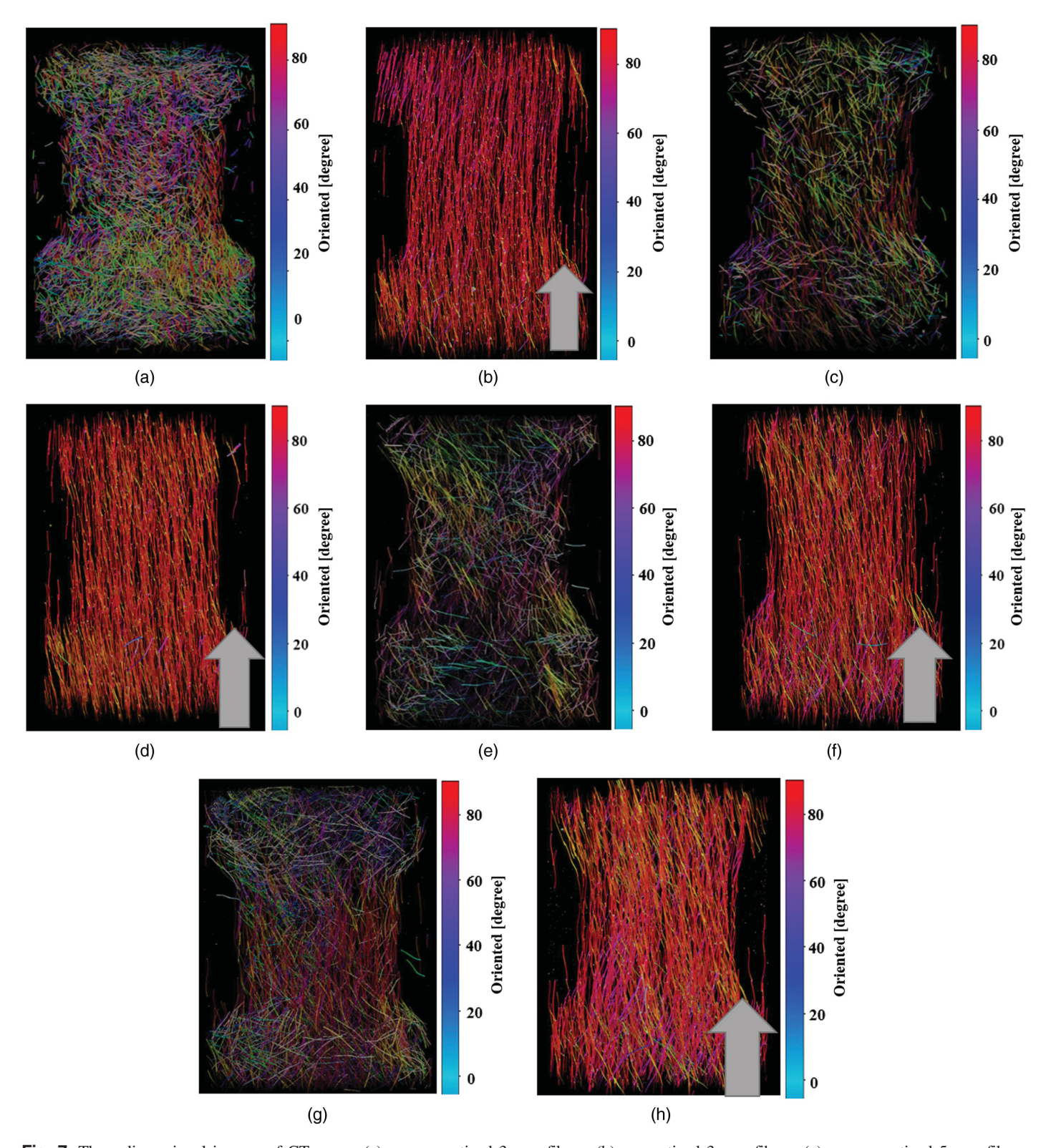


Fig. 7. Three-dimensional images of CT scans: (a) nonmagnetized 3 mm fibers; (b) magnetized 3 mm fibers; (c) nonmagnetized 5 mm fibers; (d) magnetized 5 mm fibers; (e) nonmagnetized 7 mm fibers; (f) magnetized 7 mm fibers; (g) nonmagnetized 9 mm fibers; and (h) magnetized 9 mm fibers.

a fiber fall within this range was calculated by summing the local probability of each angle. The Table 3 shows the probability of having a pixel is either 0° – 45° or 45° – 90° .

When comparing nonmagnetized to magnetized cases, it was observed that magnetization increased the probability of having a fiber pixel oriented to 45°-90° by 28.33%, 44.05%, 49.33%,

and 27.12% for the 3, 5, 7, and 9 mm fiber lengths, respectively. The largest increase was for the 7 mm fibers, with the 9 mm fibers having the smallest increase. When only considering the magnetized specimens, the 5 and 7 mm fibers had very similar distributions, while the 3 and 9 mm fibers had a slightly smaller probability of being oriented between 45° and 90°. The 5 and 7 mm

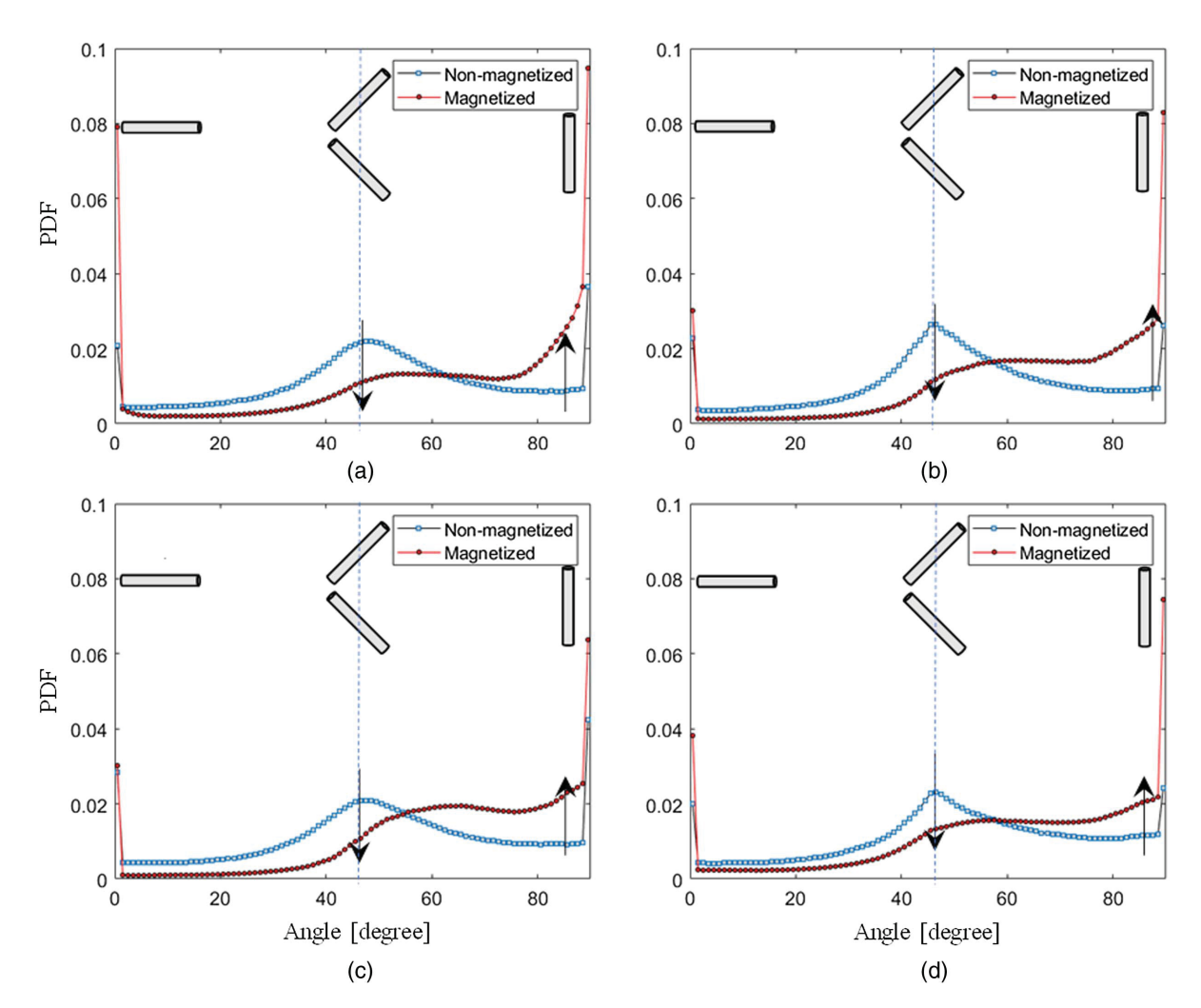


Fig. 8. Probability density functions for (a) 3 mm; (b) 5 mm; (c) 7 mm; and (d) 9 mm fibers.

Table 3. Orientation probability

Nonma		gnetized	Magn	Magnetized	
Fiber length (mm)	0–45 (degrees)	45–90 (degrees)	0–45 (degrees)	45–90 (degrees)	
3	38.42%	61.58%	23.76%	76.24%	
5	36.68%	63.32%	14.65%	85.35%	
7	37.79%	62.21%	13.16%	86.84%	
9	35.49%	64.51%	21.93%	78.07%	

fibers had a 14.65% and 13.16% probability of being oriented between 0° and 45°, respectively, and the 3 and 9 mm fibers had orientation probabilities of 23.76% and 21.93%, respectively. This implies that the 5 and 7 mm fibers were better aligned with the direction of the magnetic field. When looking at only the non-magnetized specimens, all had very similar distributions. This allowed us to accurately observe how well the fibers aligned with the magnetic field. Because all the nonmagnetized samples had very similar distributions, we could observe which fiber lengths were more susceptible to the uniform magnetic field. This study showed that the 5 and 7 mm fibers were more susceptible to the magnetic field. Besides the fibers aligned along the outside of the molds, another factor affecting the initial orientation of the fibers is the pouring method. Before being exposed to a magnetic field, the specimens were placed on a shaker table to induce the fiber

orientation. This also causes the fibers to align parallel to the length of the specimen. It should be mentioned that while other factors can affect the fiber orientation, the only difference between magnetized and nonmagnetized samples is the existence of a magnetic field. This allows us to clearly observe the effect of magnetization on the fiber orientation as well as the tensile strength.

The direct tension test results were obtained from the direct tensile testing of cylindrical SFRC specimens. These results are presented in Table 4 and Fig. 9. ACI recommends a tensile strength for concrete at 7 and 28 days of 1 MPa (150 psi) and 1.72 MPa (250 psi) (Kang and Kim 2011; Laranjeira et al. 2011; Yoo et al. 2014). Typically, UHPC exhibits compressive strengths ranging from approximately 120–175 MPa and a tensile strength of approximately 10 psi (Wille et al. 2012; Graybeal 2006).

Looking at Table 3 as well as Fig. 9, we can see that the average strength of the samples increased from 2.28 to 2.90 MPa. This is an overall increase of 27% for all samples. When looking at the individual fibers, the average tensile strengths of the 3, 5, 7, and 9 mm fibers increased by 0.51, 0.46, 0.64, and 0.76 MPa, respectively. Fig. 9 shows the Gaussian distribution of the tensile strengths of the sample, in which the red and blue lines represent the nonmagnetized and magnetized samples, respectively. It is obvious that the tensile strength of the magnetized samples increased.

Table 5 shows parameters of fitted normal distributions to the tensile results of nonmagnetized and magnetized samples. The small *P*-value indicates that the effect of magnetization on tensile

Table 4. Direct tensile test results

Fiber size		Tensile strength in (MPa)		
(mm)	Test No.	Nonmagnetized	Magnetized	% change
3	1	2.55	2.90	15
	2	1.86	2.62	39
	3	2.34	2.76	18
5	1	1.86	2.41	28
	2	2.07	2.76	33
	3	2.55	2.69	9
7	1	2.48	2.96	17
	2	2.28	2.90	30
	3	2.28	3.10	37
9	1	2.55	3.10	20
	2	1.93	3.03	57
	3	2.41	3.03	25
Average	_	2.28	2.90	27

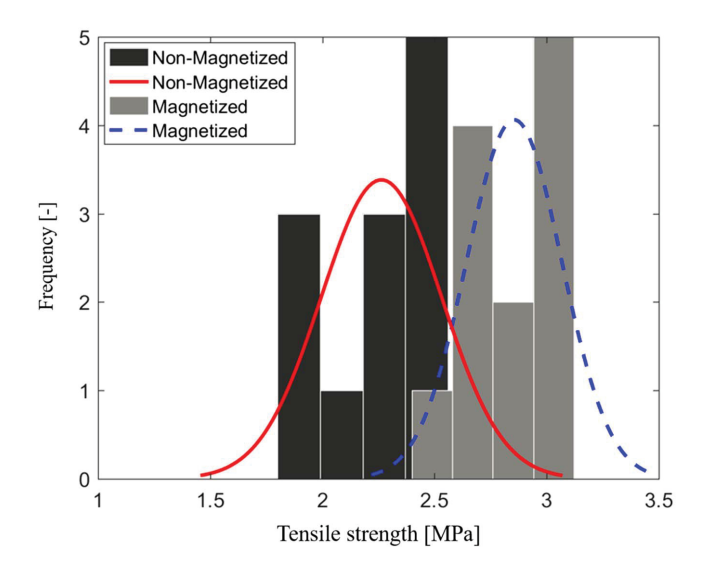


Fig. 9. Distributions of direct tension strengths for nonmagnetized and magnetized samples.

Table 5. Parameters of normal distributions fitted to tensile strength results

	Normal distribution parameters		_
Samples	Mean value (MPa)	Standard deviation	<i>p</i> -value
Nonmagnetized	2.28	0.038	
Magnetized	2.90	0.030	4.0545×10^{-6}
Change in percentage	27.00	_	_

strength is statistically insignificant. This observation shows that the tensile strength of the magnetized samples increased for all fibers. One can conclude that magnetization can substantially improve tensile strength. Consequent to the fiber alignment using magnetization, the average tensile strength substantially increased by 27%. This result showed that if fibers are aligned parallel to the direction of the tensile load in concrete materials, the required tensile strength can be obtained with less reinforcement using a lower amount of fibers, consequently resulting in more economical construction.

The use of an external magnetic field to orient fibers has important implications when considering 3D printed concrete. While steel mesh is more aligned and continuous, its applications within 3D printed concrete are limited. Applying a magnetic field to orient fibers during the printing process could be an effective way of improving the strength of the 3D printed concrete. One approach that our research team is considering is to use magnetic fields during the construction to integrate a magnetic device in a nozzle during 3D printing (Dehghan-Niri et al. 2019). A properly designed magnetic coil is needed if longer fibers are to be used, where a stronger magnetic field is required to orient the fibers properly.

This paper was focused on more quantitative analysis. While the mechanism analysis can provide additional valuable information (Ferreira et al. 2018; Mobasher et al. 1990), this analysis of the oriented fibers in the cement mortar was out of the scope of the current paper.

Conclusions

Orientation Analysis

The magnetic-based alignment of steel fibers and its effect on tensile strength in aligned steel-reinforced cementitious composites (ASFRC) were investigated in this study. The orientation of the steel fibers for the specimens was evaluated both qualitatively and quantitatively using X-ray CT scans. Using CT scans, an accurate assessment of the magnetic field used to orient the fibers could be made, along with the effects of varying the fiber length. The orientation distributions were calculated for both the magnetized and nonmagnetized samples using a gradient-based image processing method. Each nonmagnetized specimen exhibited a nonuniform distribution of fiber orientations. Compared to the magnetized specimens, an overwhelming majority of fibers were aligned with the direction of the magnetic field. This was evident in both qualitative and quantitative analyses. Based on the quantitative analysis of the orientation data, the probability of a fiber being aligned parallel to the length of the specimen increased by 28.33%, 44.05%, 49.33%, and 27.12% for fibers with lengths of 3, 5, 7, and 9 mm, respectively. In addition, it was observed that the 3 and 9 mm length fibers had the lowest probability of being aligned within the direction of the magnetic field, while the 5 and 7 mm fibers showed the highest probability.

When considering the 3 and 9 mm fibers, a couple of reasons could result in them being less susceptible to the magnetic field than the 5 and 7 mm fibers. When exposed to a magnetic field, the two main forces acting on the fibers are the resulting magnetic force and viscous resistance. When the fibers are short, the effect of the magnetic field is not as strong as the longer fibers. However, when the length of the fibers is increased, the viscous resistance will also increase. Thus, it was concluded that the fiber length is directly related to the orientation of the fibers in the direction of the magnetic field. If the fibers are too short, the magnetic field will not have a strong enough effect to orient them effectively. However, if the fibers are too long, the viscous resistance of the cement mortar will be strong enough to impair their rotation.

Tensile Strength

The average tensile strength of the samples increased from 2.25 to 2.76 MPa, 2.16 to 2.62 MPa, 2.34 to 2.98 MPa, and 2.29 to 3.05 MPa for the 3, 5, 7, and 9 mm fiber lengths, respectively. On average, the tensile strength of the samples increased by 27% after being exposed to an external magnetic field. The tensile strength of the samples increased substantially for all the specimens after

magnetization. The average tensile strength increased by 27% owing to fiber alignment in the ASFRC samples. This shows that if the ASFRC fibers are aligned parallel to the direction of the tensile load, the tensile capacity of the concrete will increase, resulting in superior tensile performance without increasing the number of steel fibers. Notice that the sample containing 5 mm fibers increased by the least amount. This is a special case in which the general trend shows that tensile strength increases with the increasing fiber length.

The results for each fiber length contain uncertainties due to the testing machine, the molding and curing process, and so forth, so that three samples might not be considered statistically significant. However, the total number of samples (15) adequately shows the relationship between fiber orientation and tensile strength.

Data Availability Statement

Some or all data, models, or code that support the findings of this study are available from the corresponding author upon reasonable request.

Acknowledgments

Computed tomography work was supported by the US National Science Foundation (Grant No. 1840138).

References

- ASTM. 2007. Standard test method for flow of hydraulic cement mortar. ASTM C1437. West Conshohocken, PA: ASTM.
- ASTM. 2013. Tensile strength of concrete surfaces and the bond strength. ASTM C1583. West Conshohocken, PA: ASTM.
- Barnett, S. J., J. F. Lataste, T. Parry, S. G. Millard, and M. N. Soutsos. 2010. "Assessment of fibre orientation in ultra high performance fibre reinforced concrete and its effect on flexural strength." *Mater. Struct.* 43 (7): 1009–1023. https://doi.org/10.1617/s11527-009-9562-3.
- Chen, H. J., Y. L. Yu, and C. W. Tang. 2020. "Mechanical properties of ultra-high performance concrete before and after exposure to high temperatures." *Materials (Basel)* 13 (3): 1–17. https://doi.org/10.3390 /ma13030770.
- Chu, S. H. 2019. "Effect of paste volume on fresh and hardened properties of concrete." Constr. Build. Mater. 218 (Sep): 284–294. https://doi.org /10.1016/j.conbuildmat.2019.05.131.
- Chu, S. H., and A. K. H. Kwan. 2019. "A new bond model for reinforcing bars in steel fibre reinforced concrete." *Cem. Concr. Compos.* 104 (Nov): 103405. https://doi.org/10.1016/j.cemconcomp.2019.103405.
- Ciambella, J., D. C. Stanier, and S. S. Rahatekar. 2017. "Magnetic alignment of short carbon fibres in curing composites." *Composites, Part B* 109 (Jan): 129–137. https://doi.org/10.1016/j.compositesb.2016.10 .038.
- Darwin, D., C. W. Dolan, and A. H. Nilson. 2016. Design of concrete structures. New York: McGraw-Hill.
- Dehghan-Niri, E., B. Weldon, and R. Foudazi. 2019. *Electromagnetic-based multi-directional alignment method and apparatus for fibers in composite materials*. Pending US Patent Application 16/866,490. Washington, DC: US Patent and Trademark Office.
- Edgington, J., and D. J. Hannant. 1972. "Steel fiber reinforced concrete. The effect on fibre orientation of compaction by vibration." *Mater. Constr.* 5 (1): 41–44. https://doi.org/10.1007/BF02479076.
- Ferreira, S. R., M. Pepe, E. Martinelli, F. de Andrade Silva, and R. D. Toledo Filho. 2018. "Influence of natural fibers characteristics on the interface mechanics with cement based matrices." *Composites, Part B* 140 (May): 183–196. https://doi.org/10.1016/j.compositesb.2017.12.016.

- Garcia, E. Y. F. 2019. "Bond strength assessment of ultra-high performance concrete for shear key applications in concrete bridges." Ph.D. thesis, Dept. of Civil Engineering, New Mexico State Univ.
- Gonzalez, R., and R. Woods. 2008. *Digital image processing*. New York: Pearson.
- Graybeal, B. A. 2006. Material property characterization of ultra-high performance concrete. Rep. No. FHWA-HRT-06-103. Washington, DC: Federal Highway Administration, Office of Infrastructure Research and Development.
- Groeneveld, A. B., T. M. Ahlborn, C. K. Crane, and W. R. Long. 2017.
 Effect of fiber orientation on dynamic compressive properties of an ultra-high performance concrete. ERDC/GSL TR-17-23. Washington, DC: Transportation Research International Documentation.
- Gyawali, S. R. 2008. "Design and construction of Helmholtz coil for biomagnetic studies on soybean." M.S. thesis, Dept. of Electrical Engineering. Univ. of Missouri–Columbia.
- Islam, N. E. 2008. "Design and construction of Helmholtz Coil for biometric for biomagnetic studies on soybean." Master thesis, Dept. of Electrical Engineering, Univ. of Missouri-Columbia.
- Juárez-Badillo, E. 1999. "Stress-strain relationship of confined high-strength plain and fiber concrete." J. Mater. Civ. Eng. 11 (4): 363. https://doi.org/10.1061/(ASCE)0899-1561(1999)11:4(363).
- Kang, S. T., and J. K. Kim. 2011. "The relation between fiber orientation and tensile behavior in an ultra high performance fiber reinforced cementitious composites (UHPFRCC)." Cem. Concr. Res. 41 (10): 1001–1014. https://doi.org/10.1016/j.cemconres.2011.05.009.
- Kim, S. W., S. T. Kang, J. J. Park, and G. S. Ryu. 2008. "Effect of filling method on fibre orientation & dispersion and mechanical properties of UHPC." In *Proc.*, 2nd Int. Symp. on UHPC, 185–195. Kassel, Germany: Kassel University Press.
- Kimura, T., M. Yamato, W. Koshimizu, M. Koike, and T. Kawai. 2000. "Magnetic orientation of polymer fibers in suspension." *Langmuir* 16 (2): 858–861. https://doi.org/10.1021/la990761j.
- Kwan, A. K. H., and S. H. Chu. 2018. "Direct tension behaviour of steel fibre reinforced concrete measured by a new test method." *Eng. Struct*. 176 (Dec): 324–336. https://doi.org/10.1016/j.engstruct.2018.09.010.
- Laranjeira, F., A. Aguado, C. Molins, S. Grünewald, J. Walraven, and S. Cavalaro. 2012. "Framework to predict the orientation of fibers in FRC: A novel philosophy." *Cem. Concr. Res.* 42 (6): 752–768. https://doi.org/10.1016/j.cemconres.2012.02.013.
- Laranjeira, F., S. Grünewald, J. Walraven, C. Blom, C. Molins, and A. Aguado. 2011. "Characterization of the orientation profile of steel fiber reinforced concrete." *Mater. Struct.* 44 (6): 1093–1111. https://doi.org/10.1617/s11527-010-9686-5.
- Li, H., R. Mu, L. Qing, H. Chen, and Y. Ma. 2018. "The influence of fiber orientation on bleeding of steel fiber reinforced cementitious composites." *Cem. Concr. Compos.* 92 (May): 125–134. https://doi.org/10.1016/j.cemconcomp.2018.05.018.
- Lutz, M. 2013. Learning Python. 5th ed. Sebastopol, CA: O'Reilly Media. Mobasher, B., A. Castro-Montero, and S. P. Shah. 1990. "A study of fracture in fiber-reinforced cement-based composites using laser holographic interferometry." Exp. Mech. 30 (3): 286–294. https://doi.org/10.1007/BF02322824.
- Mortazavian, S., and A. Fatemi. 2015. "Effects of fiber orientation and anisotropy on tensile strength and elastic modulus of short fiber reinforced polymer composites." *Composites, Part B* 72 (Apr): 116–129. https://doi.org/10.1016/j.compositesb.2014.11.041.
- Mu, R., H. Li, L. Qing, J. Lin, and Q. Zhao. 2017. "Aligning steel fibers in cement mortar using electro-magnetic field." *Constr. Build. Mater*. 131 (Jan): 309–316. https://doi.org/10.1016/j.conbuildmat.2016.11 .081.
- Püspöki, Z., M. Storath, D. Sage, and M. Unser. 2016. "Transforms and operators for directional bioimage analysis: A survey." In *Focus on bio-image informatics*, 69–93. Cham, Switzerland: Springer.
- Reddy, B. S. K., V. G. Ghorpade, and H. S. Rao. 2013. "Effect of magnetic field exposure time on workability and compressive strength of magnetic water concrete." *Int. J. Adv. Eng. Technol.* 4 (3): 120–122.
- Stähli, P., R. Custer, and J. G. M. Van Mier. 2008. "On flow properties, fibre distribution, fibre orientation and flexural behaviour of FRC." *Mater. Struct.* 41 (1): 189–196. https://doi.org/10.1617/s11527-007-9229-x.

- Subburaj, K. 2012. CT scanning: Techniques and applications. Rijeka, Croatia: InTech.
- Villar, V. P., N. F. Medina, M. M. Alonso, S. G. Diez, and F. Puertas. 2019a. "Assessment of parameters governing the steel fiber alignment in fresh cement-based composites." *Constr. Build. Mater.* 207 (May): 548–562. https://doi.org/10.1016/j.conbuildmat.2019.02.036.
- Villar, V. P., N. F. Medina, and F. Hernández-Olivares. 2019b. "A model about dynamic parameters through magnetic fields during the alignment of steel fibres reinforcing cementitious composites." *Constr. Build. Mater.* 201 (Mar): 340–349. https://doi.org/10.1016/j.conbuildmat.2018.12.105.
- Wijffels, M. J. H. 2013. "Magnetically orienting steel fibres in self-compacting concrete." Ph.D. thesis, Dept. of the Built Environment, Eindhoven Univ. of Technology.
- Wijffels, M. J. H., R. J. M. Wolfs, A. S. J. Suiker, and T. A. M. Salet. 2017. "Magnetic orientation of steel fibres in self-compacting concrete beams: Effect on failure behaviour." *Cem. Concr. Compos.* 80 (Jul): 342–355. https://doi.org/10.1016/j.cemconcomp.2017.04.005.
- Wille, K., A. E. Naaman, S. El-Tawil, and G. J. Parra-Montesinos. 2012. "Ultra-high performance concrete and fiber reinforced concrete: Achieving strength and ductility without heat curing." *Mater. Struct.* 45 (3): 309–324. https://doi.org/10.1617/s11527-011-9767-0.
- Xue, W., J. Chen, F. Xie, and B. Feng. 2018. "Orientation of steel fibers in magnetically driven concrete and mortar." *Materials (Basel)* 11 (1): 1–12. https://doi.org/10.3390/ma11010170.

- Yoo, D. Y., N. Banthia, S. T. Kang, and Y. S. Yoon. 2016. "Effect of fiber orientation on the rate-dependent flexural behavior of ultra-high-performance fiber-reinforced concrete." *Compos. Struct.* 157 (Dec): 62–70. https://doi.org/10.1016/j.compstruct.2016.08.023.
- Yoo, D. Y., S. T. Kang, and Y. S. Yoon. 2014. "Effect of fiber length and placement method on flexural behavior, tension-softening curve, and fiber distribution characteristics of UHPFRC." Constr. Build. Mater. 64 (Aug): 67–81. https://doi.org/10.1016/j.conbuildmat.2014.04 .007.
- Zhang, P., Q. Li, Y. Chen, Y. Shi, and Y. F. Ling. 2019. "Durability of steel fiber-reinforced concrete containing SiO₂ nano-particles." *Materials* (Basel) 12 (13): 2184. https://doi.org/10.3390/ma12132184.
- Zhang, P., Y. N. Zhao, Q. F. Li, T. H. Zhang, and P. Wang. 2014a. "Mechanical properties of fly ash concrete composite reinforced with nano-SiO₂ and steel fibre." *Current Sci.* 106 (11): 1529–1537.
- Zhang, P., Y. N. Zhao, C. H. Liu, P. Wang, and T. H. Zhang. 2014b. "Combined effect of nano-SiO₂ particles and steel fibers on flexural properties of concrete composite containing fly ash." Sci. Eng. Compos. Mater. 21 (4): 597–605. https://doi.org/10.1515/secm-2013-0179.
- Zhou, B., and Y. Uchida. 2013. "Fiber orientation in ultra high performance fiber reinforced concrete and its visualization." In *Proc.*, 8th Int. Conf. on Fracture Mechanics of Concrete and Concrete Structures, 228–235. Gifu, Japan: Gifu Univ.